


ITC 2/51 Information Technology and Control Vol. 51 / No. 2 / 2022 pp. 332-344 DOI 10.5755/j01.itc.51.2.30835	A Deep Transfer Learning Based Architecture for Brain Tumor Classification Using MR Images	
	Received 2022/03/02	Accepted after revision 2022/05/11
	 http://dx.doi.org/10.5755/j01.itc.51.2.30835	

HOW TO CITE: Badjie, B., Ülker, E. D. (2022). A Deep Transfer Learning Based Architecture for Brain Tumor Classification Using MR Images. *Information Technology and Control*, 51(2), 332-344. <http://dx.doi.org/10.5755/j01.itc.51.2.30835>

A Deep Transfer Learning Based Architecture for Brain Tumor Classification Using MR Images

Bakary Badjie, Ezgi Deniz Ülker

Faculty of Engineering; European University of Lefke; Mersin-10, Turkey,
e-mails: bakarykumba1996@gmail.com, eulker@eul.edu.tr

Corresponding author: eulker@eul.edu.tr

Deep Learning (DL) is becoming more popular in the healthcare sectors due to the exponential growth of data availability and its excellent performance in diagnosing various diseases. This paper has aimed to design a new possible brain tumor diagnostic model to improve accuracy and reliability of radiology. In this paper, an advanced deep learning algorithm is used to detect and classify brain tumors in magnetic resonance (MR) images. Diagnosing brain tumors in radiology is a significant issue, yet it is a difficult and time-consuming procedure that radiologists must pass through. The reliability of their assessment relies completely on their knowledge and personal judgements which are in most cases inaccurate. As a possible remedy to the growing concern in diagnosing brain tumors accurately, in this work a deep learning method is applied to classify the brain tumor MR images with very high performance accuracy. The research leveraged a transfer learning model known as AlexNet's convolutional neural network (CNN) to perform this operation. Our method helps to improve robustness, efficiencies and accuracy in the healthcare sector with the ability to automate the entire diagnostic process with the overall accuracy of 99.62%. Additionally, our model has the ability to detect and classify tumors at their different stages and magnitudes.

KEYWORDS: Artificial neural networks, Image classification, Learning systems, Magnetic resonance imaging, Tumors.

1. Introduction

Recent innovations, particularly in the areas of artificial intelligence (AI) and machine learning (ML), have had a considerable influence on radiology, serving as both a vital supportive approach and transformative solutions in this domain. In MR image processing, several machine-learning algorithms for the segmentation and classifications of images are used to offer a rapid diagnosis in brain tumors with high accuracy to the radiologists. A brain tumor is the development of additional cells in the brain that is aberrant and affects roughly 350,000 people globally annually. There are about 145 different varieties of brain tumors that have been discovered and are divided into two groups; primary brain tumors that develop in the brain tissue and spread to other areas of the body and secondary or metastatic brain tumors that start in other regions of the body and expand to the brain. This illness is fatal and can prevent proper growth of the brain, mainly in people under the age of nine. The annual report of the National Cancer Institute in America shows that more than 30,500 brain tumor patients were identified of which 17,125 were males and 13,375 were women and 13,700 of these patients lost their lives in the year 2020 [3]. Moreover, evaluation and analysis of a massive MR image dataset is challenging for humans. The ability of radiologists to diagnose brain tumors at an early stage is solely dependent on their expertise. However, diagnosing brain tumors cannot be accomplished without determining, if the tumor is a benign or a malignant tumor prior to final surgery, unlike tumors in other parts of the body [3]. Therefore, deep learning can be used to provide accurate diagnosis during surgical operations [12]. For image analysis and classification, different deep learning techniques and versions of transfer learning have been proposed in the literature [3, 8-12, 20, 30].

Several clinical datasets have been used to evaluate these alternative methods, including MRI scans of brain tumor and tumors from various regions of the human body. Cheng et al. [8] was the first presenter of this dataset that we utilized in this study. Their feature extraction and classification techniques were based on the use of a pre-trained deep learning model and they achieved a performance accuracy of 91.28%. Deepak and Ameer [10] employed an already-trained GoogLeNet model to extract the most important fea-

tures from brain MR images using a Siamese Neural Network (SNN) and achieved 97.64% accuracy in classifying three kinds of brain tumors. Diaz-Pernas et al. [11] introduced a multi-scale CNN design for automated glioma, meningioma, and pituitary tumor segmentation. They tested their model against a publicly accessible T1-weighted counterpoint MRI dataset and found it to be 97.3% accurate. Adopting a genetic algorithm and a support vector machine (SVM), Kharrat et al. [20] divided brain tumors into normal and pathological categories and they claimed an accuracy of 98.14%. Preethi and Aishwarya [30] suggested a strategy for categorizing brain tumors into phases. The feature matrix was created by combining the adaptive filtering-based gray-level co-occurrence matrix with GLCM, combined with deep neural network and they claimed an accuracy of 99.3%. To categorize the brain MR images, Cinar and Yildirim [9] employed several CNN architectures such as GoogLeNet, Inception-V3, DenseNet201, AlexNet and ResNet50 and obtained accurate results. They changed an already-trained ResNet50 CNN by eliminating its final five layers and adding new eight layers resulting in a model with 97.2% accuracy, the best among all pre-trained models they used in their work. Using a dataset of 428 brain MR images, Kumar and Vijayakumar [23] proposed a method combined with a kernel-based SVM algorithm for detecting and segmenting tumors in the human brain, achieving 95.98%, 95% overlap fraction and 0.025% additional fraction. AlexNet was the first transfer learning model which was created [4]. After that inspiring work researchers were motivated and other transfer learning models were invented such as ResNet50, VGG19, VGG16, GoogLeNet, Inception-V3. Geoffrey Hinton, who is the father of backpropagation, his idea of backpropagation led to the advancement of Deep Learning (DL) [25]. DL algorithms in radiology demonstrate excellent performance compared to Machine Learning (ML) algorithms due to the exponential growth in data [1, 5, 14, 27, 35]. The performance of deep learning algorithms increases as the amount of data increases, meanwhile the performance of machine learning algorithms almost stays steady.

Another reason of the popularity of DL is technological advancement, which is critical because there is powerful hardware such as NVidia, GPUs, Jetson

Nano which allows us to easily train any type of deep learning model on a massive network. One of the most important factors that also led to the growth of deep learning is the technique of transfer learning. This is quite a useful technique in deep learning as it allows us to use the knowledge of a pre-existing model that has been trained on a massive dataset for our problem statement. This technique accelerates the process with less computational power required during training [18]. Essentially, deep learning is a subset of machine learning that enables machines or computers to mimic how human beings learn. It is an important feature of data science that encompasses statistical and predictive analytics to train a huge amount of data using deep layers. There are various radiographic techniques that DL uses to perform tumor diagnostics. Some of these imaging techniques are; Magnetic Resonance Imaging scans (MRI), Computerized Tomography scans (CT), Mammography Scans, Nuclear Medicine scans and Positron Emission Tomography (PET) among others [29]. There are many capital and human resources that have been invested in this area since its introduction in radiology.

This paper proposes CNN architecture to detect and classify the brain tumors using MR images with high performance accuracy. The parameters of the AlexNet model were transferred to a new CNN model where the top layers were frozen and the new dense layers were added for the better classification. By modifying the CNN model, our new method has the capability to detect the number of unhealthy MR images among the healthy MR images in the dataset. This technique automates the entire diagnostic process and optimizes the workflow of the radiologist. Detecting and classifying the brain tumors requires high level of human effort and it is almost impossible for a radiologist to correctly identify tumors in thousands of brain MR images at the same time [2]. In this study, the prime objective is to design a deep transfer learning model with an improved accuracy.

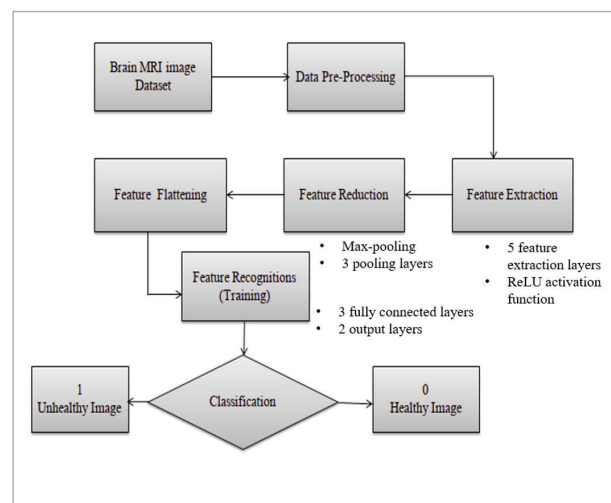
The rest of the paper is organized as follows; Section 2 elaborates the proposed method with the architectural details. The information of the network parameters and the data set used in the experiments were mentioned in this section. Section 3 discusses the results of the several experimental studies of our model with some state-of-art algorithms in the literature followed by a conclusion in Section 4.

2. Methodology

Our aim is to analyze the entire diagnostic process in detecting and classifying the brain tumors in various stages and magnitudes. Figure 1 illustrates the entire process of the proposed technique for diagnosing brain tumors. The implementation starts with obtaining the brain MRI dataset. It is applied through some data preparation techniques such as exploratory data analysis, data wrangling and feature engineering in order to extract the necessary parts of the data and to observe the correlations between the data points. After this process, the pre-processed data is fed into the convolutional layer of our network which extracts the important features of the data. Some of the features of the data are reduced by the feature reduction layer known as the max-pooling layer [13], before they are flattened up into one-dimensional vectors by the flattening layer. Feature recognition is carried out by the fully-connected dense layers during the training process. Classification is done at the last layer of the network which is known as the decision-making layer. This layer outputs the results of the prediction on the data, whereas in our case, 1 indicates that an image contains a tumor and 0 indicates that an image does not contain tumor. These results are matched with the ground truth labels for evaluation purposes.

Figure 1

Flowchart of the overall classification design for the proposed model

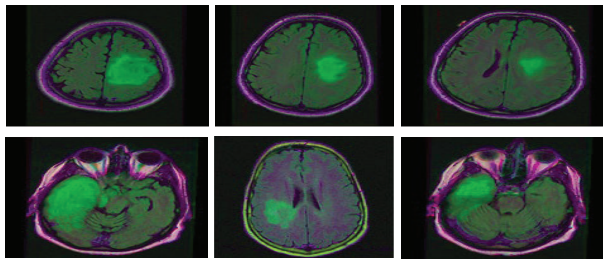


A. Image Database

The Kaggle database was used to collect the dataset (BraTS2020 Dataset) for this research [16]. The data consists of 3929 brain MR image samples where 2756 were identified as tumor-affected images and 1173 samples were identified as non-tumor-affected. The dataset contains two tumor types. 1290 images are malignant tumors and 1466 images are benign tumors. In all, 3929 patients' brain tumor images were collected between 2005 and 2010 through MRI scan technology. It was initially released in 2015 on the Kaggle database and the most recent update was in 2021 [16]. This indicates that the classification task in this study was performed on an unbalanced dataset. Different types of tumors in different planes and magnitudes are shown in Figure 2 where the tumor is indicated by a dark-green edge.

Figure 2

Example MR images from the dataset used in experiments



B. Data Pre-processing and Augmentation

MRI data samples from our database come in various sizes and are presented in 16-bit signed integer (int16) format. In order to match with the input of our CNN

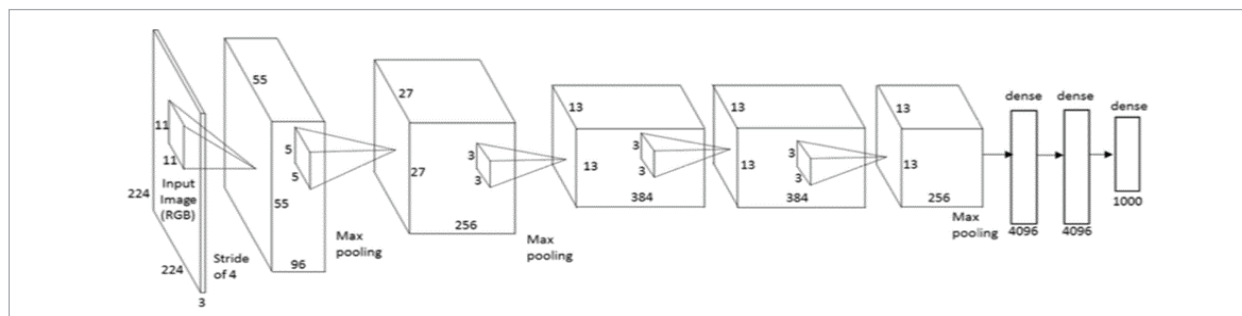
network, all the images in our dataset must be resized to 224 by 224 pixels. First, all the images are normalized and resized to meet the requirements of the input layer of our network to perform a possible feature extraction on our images. For possible data augmentation, we performed only one image transformation technique. The images were rotated by 90 degrees and we concatenated them to the original dataset, so the total images became 7858 samples. The augmented images are 3929 and the original images are also 3929. Concatenating them together resulted in 7858 image samples, which were used in our experiment. Image augmentation is an important technique in image pre-processing and it enables us to acquire more data required for any deep and machine learning. It also helps to reduce the biasness of the model [28].

C. Network Architecture

This paper proposes model that detects and classifies brain tumors with the help of a pre-existing model known as AlexNet [4]. The detection and classification was done using Python with Google Colab as an Integrated Development Environment (IDE). AlexNet is a transfer learning with an input layer which is represented by an image dataset, 5-feature extraction blocks, 3-feature reduction layers and 3-fully-connected dense layers known as the classification block and finally 2-output layers. This architecture was initially designed by Alex Krizhevsky and supervised by Geoffrey Hinton [22]. The architecture has 1000 outputs because it was initially designed on an ImageNet dataset which consists of 1000 different categories and over 11 million image samples. This network was the first advanced CNN model to win the ImageNet competition with a top-5 error of 15.3% in 2012. Figure 3 demonstrates the design of this network [33].

Figure 3

AlexNet CNN architecture [33]



In this paper, the parameters of the AlexNet network were transferred to a new CNN network and the top layers were frozen, then new dense or full-connected layers were added. The reason for adopting this architecture is that its parameters were previously trained on millions of images and perform well on a similar task. Using these pre-trained parameters reduced training time, computational power and improved model performance accuracy. After adding new dense layers, we achieved around 91 million trainable parameters, as shown in Table 1. These trainable parameters performed effectively on the dataset used in the experiment. The properties of the layers of our network with their corresponding values are elaborated in Table 2.

Table 1

The number of parameters of the network

Parameters	
Total Parameters	91,782,754
Trainable Parameters	91,761,614
Non-trainable Parameters	21,140

In this architecture, each convolutional block has a feature extraction layer, a batch normalization layer, a rectified linear unit (ReLU) activation layer and a dropout layer [26]. With the exception of the third and fourth convolutional layers, each convolutional block is followed by a max-pooling or down-sampling layer.

The convolutional or feature extraction layers execute convolution operations on the images by performing pixel-wise multiplications, extracting the most important features from the images with a given number of kernel filters, striding and padding [26]. Convolution is defined as follows;

$$B(i, j) = \sum_m \sum_n K(m, n) * A(i - m, j - n), \quad (1)$$

where K is the convolution kernel in size (m, n) , A is the image is size (i, j) and B is the output image of the convolution in size (i, j) . Figure 4 shows the convolved features of the MR images after the convolutional layers. These layers have different kernel filters which have the ability to detect and extract the important features from the original images before down-sampling the images. By enabling the weights

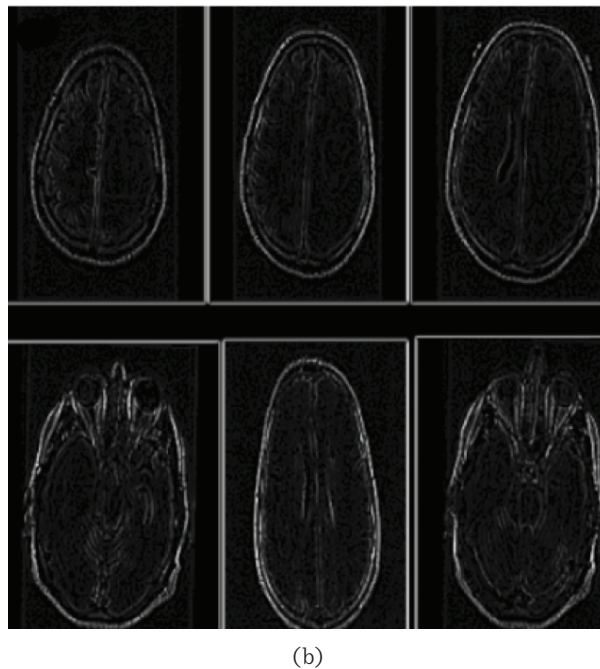
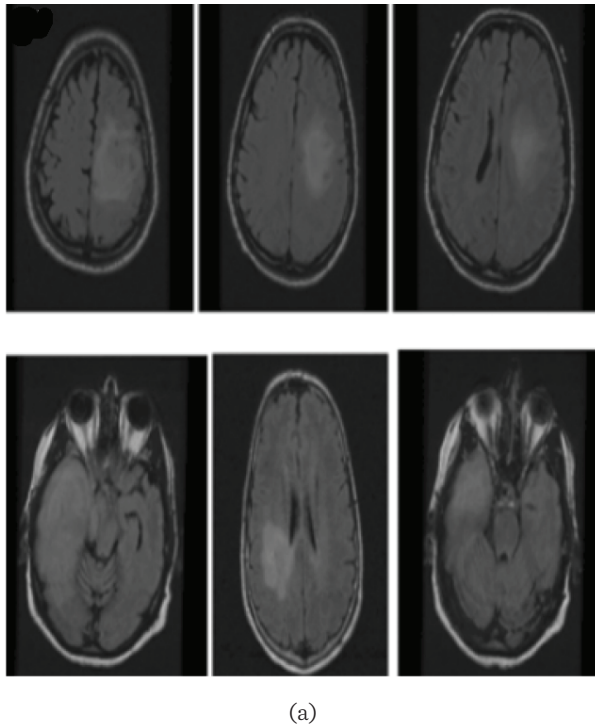
Table 2

Layer properties of our proposed network

Layer Name	Layer Properties
Image Input	256 × 256 × 1 images
1st Convolutional Block Convolutional Layer Rectified Linear Unit layer Batch Normalization	Kernel filter=96, Kernel size=[11x11], strides=[4x4], padding='same' ReLU activation function Batch Normalization
Max-pooling Layer	Pooling Size=[4 x4], stride=[2x2], padding=0
2nd Convolutional Block Convolutional Layer Rectified Linear Unit layer Batch Normalization	Kernel filter=256, Kernel size=[5x5], strides=[1x1], padding='same' ReLU activation function Batch Normalization
Max-pooling Layer	Pooling Size=[4 x4], stride=[2x2], padding=0
3rd Convolutional Block Convolutional Layer Rectified Linear Unit layer Batch Normalization	Kernel filter=384, Kernel size=[3x3], strides=[1x1], padding='same' ReLU activation function Batch Normalization
4th Convolutional Block Convolutional Layer Rectified Linear Unit layer Batch Normalization	Kernel filter=384, Kernel size=[3x3], strides=[1x1], padding='same' ReLU activation function Batch Normalization
5st Convolutional Block Convolutional Layer Rectified Linear Unit layer Batch Normalization	Kernel filter=256, Kernel size=[3x3], strides=[1x1], padding='same' ReLU activation function Batch Normalization
Max-pooling Layer	Pooling Size=[4 x4], stride=[2x2], padding=0
1st Classification Block Fully-connected Layer Activation layer Dropout	Hidden neurons=4096 neurons ReLU activation function 40 percent
2nd Classification Block Fully-connected Layer Activation layer Dropout	Hidden neurons=4096 neurons ReLU activation function 40 percent
3rd Classification Block Fully-connected Layer Activation layer Dropout	Hidden neurons=4096 neurons ReLU activation function 40 percent
Output Layer Dense Layer Activation layer	2 Neurons. These neurons gave us the predictive outputs. Sigmoid

Figure 4

Brain Tumor images using MRI scan. The original image is illustrated in (a) after converting it to one-dimension gray scale while in (b) convolved features after passing through the convolutional layers of our model



to be updated without encountering vanishing gradient issues during training, the ReLU activation layer provides an activation function that supports effective back-propagation. The dropout layer is used to prevent the network from over-fitting by dropping some weights with their corresponding neurons [34]. ReLU activation function is defined as follows;

$$Y_i = \max(x, 0) \text{ and } x = w_i x_i + b_i, \tag{2}$$

where w is the weight of the network in size, x is the input image, b is the bias term and Y is the ReLU activation function.

The max-pooling layer samples the output features from the convolutional block and applies a pooling filter with a specified number of striding. This reduces the features by selecting the highest pixel values for optimization purposes [31]. An example of max pooling is shown in the Figure 5 where stride size is $[2 \times 2]$ and pooling size is $[4 \times 4]$. It employs a location-invariant down-sampling process, where a pooling filter is applied to the convolved feature from the convolutional layer and the highest pixel value. Down-sampling is defined as follows;

$$I(x, y) = \left\lfloor \frac{A_{x,y-P}}{s} \right\rfloor, \tag{3}$$

where I is the down-sampled features, A is the convolved features with the coordinates x and y , P is pooling filter and S denotes the strides. Figure 6 shows the features of the MR images after the down-sampling process. After the convolved features were extracted from the images, the features were passed into a max-pooling layer which down-sampled the images using pooling or down-sampling filters. This reduces the size of the images by considering only the maximum pixel values as their output features.

Figure 5

Max pooling process using the pool size $[4 \times 4]$ and the stride $[2 \times 2]$

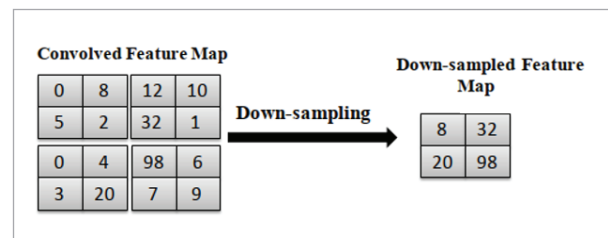
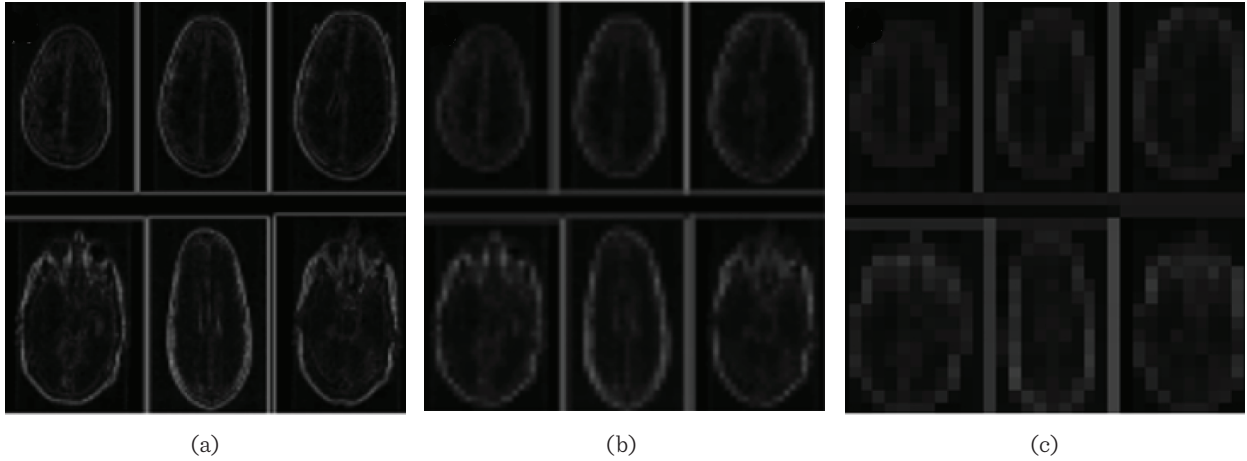


Figure 6

The convolved features of the image are illustrated after the first pooling layer in (a) while in (b) after the second pooling layer and in (c) after the final pooling layer



After the final max-pooling, the images are passed into a flatten layer which flattens the images into one-dimensional feature vectors before they are fed into the dense, fully-connected network [7]. The second phase of the network's architecture is the fully-connected layer which is made up of nodes or neurons which are connected together by lines called weights.

This layer receives the feature vectors from the corresponding flatten layer and it performs the classification on the images. It works based on two important principles which are forward and backward propagation. It is expressed as follows;

$$y_i^{(l)} = f(z_i^{(l)}) \text{ and } z_i^{(l)} = \sum_{j=1}^{m_1^{(l-1)}} w_{ij}^{(l)} y_j^{(l-1)}, \quad (4)$$

where m_1 and m_2 are flatten feature vectors, $y_i^{(l)} = f(z_i^{(l)})$ is the fully connected layer and w is the weight. This layer also tuned the weight parameters $w_{ij}^{(l)}$ in order to generate a stochastic probability representation of each class centered on the activation maps produced by the sum of convolutional, non-linearity, rectification and pooling layers. At the end of these processes, the output layer which provides the predictive analysis and evaluation of the model is achieved.

D. Training the Network

According to the previous research, when the training datasets are small, a difficulty arises on applying

the deep learning and training CNN [36]. Moreover, splitting the datasets into multiple groups has a good impact on the performance and some researchers used this method in splitting the data into three sets [6, 17, 34]. The entire dataset is divided into 80% for training, 10% for testing and 10% for validation sets respectively before being fed to the model. In this way, it is ensured that the final model evaluation is performed using a test dataset which has not been used prior, either for training the model or tuning the model parameters [21, 32]. Considering the size of the data set, by using this approach, a good performance evaluation can be obtained at a low computational cost.

By updating the model in response to the loss values, Adam optimizer was employed to help reduce the loss after each iteration or epoch [19]. Binary cross-entropy loss is used as a cost function which allows us to keep track of the model's behavior throughout the training. It aids in determining the proximity of the model to the global minima point on the gradient descent curve by comparing each of the predicted. It aids in the understanding of the model's nature by computing the model's loss at each epoch. The binary cross-entropy loss function is described as follows;

$$B(y) = -y * \log(\hat{y}) - (1 - y) * \log(1 - \hat{y}), \quad (5)$$

where y represents the actual values and \hat{y} represents the predicted values.

This process is supported by backpropagation where a bunch of chain rules occur to find the global minima on the gradient curve. A learning rate of 0.001 is used to show the degree of the trend the model is learning and it also helps in updating the weights during backpropagation. However, early-stopping was applied to stop the training process after 20 epochs, if the model was diverging from the global minima on the tangent line [7, 24]. In addition, we used a batch size of 100 images and 40 epochs for this training.

3. Experimental Results and Discussions

In this section, the results of the experiments and the performance of the model during and after the training are given. Upon completing the training process, the model was tested and evaluated on a test dataset where an effective performance was achieved with the accuracy 99.62%. This shows that the model has learned adequately without over-fitting or memorizing the training data. In another saying, during the learning process the model has gone through each and every data point without skipping any of the data points. The confusion matrix and its parameters which were used to evaluate the model are shown in Figure 7 and Table 3, respectively. According to the confusion matrix, True Positive (TP) and True Negative (TN) show the number of samples correctly classified by the model in both non-tumor affected and tumor-affected image sets respectively, while the false positive and false negative indicate the number of samples misclassified by the model. All the tumor-affected images were correctly classified as tumor-affected and 2 samples from the non-tumor affected image set were classified as tumor-affected. In the same vein, 2744 samples were rightly classified as non-tumor affected out of the non-tumor affected image set.

This shows that, out of the 7858 image samples, only 2 images were misclassified by the model, which indicated that the model has learned extremely well and has an ability to classify any future dataset of this type and shape accurately. The classification report shown in Table 4 with the precision, recall and F1-score of the model tells more about its performance.

According to Table 4, the model achieved 100% Precision, 100% Recall and 100% F1-score on the non-tu-

Figure 7

Confusion matrix of the proposed network

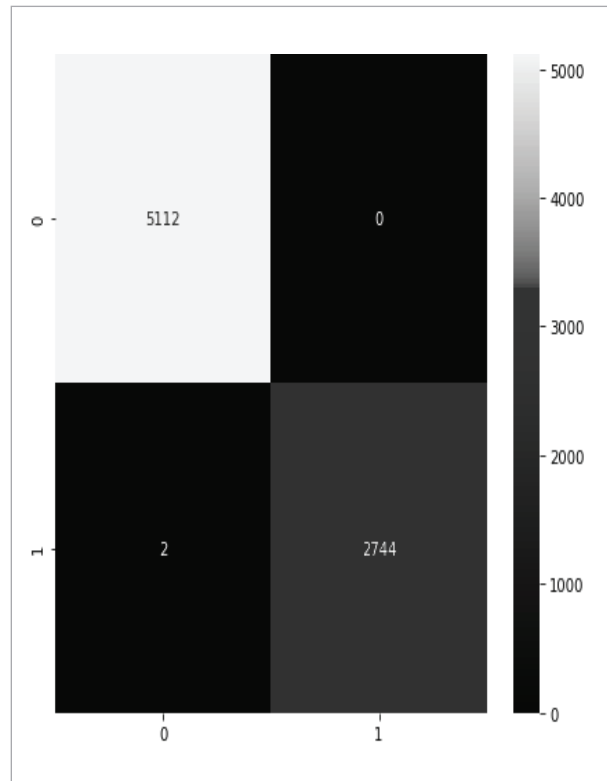


Table 3

Confusion matrix of the proposed network

True Positive (TP)	False Positive (FP)	True Negative (TN)	False Negative (FN)
5112 samples	0 samples	2744 samples	2 samples

Table 4

Classification results of the proposed network

	Precision	Recall	F ₁ -score	Support
0	1.00	1.00	1.00	502
1	1.00	0.99	0.99	278
Micro avg	1.00	1.00	1.00	780
Macro avg	1.00	1.00	1.00	780
Weighted avg	1.00	1.00	1.00	780

mor affected images while it achieved 100%, 99% and 99% Precision, Recall and F1-score on the tumor affected images, respectively. The Precision shows that the model has an ability to identify only the relevant data points during training and Recall shows its ability to find relevant instances in the dataset. F1-score demonstrates the harmonic mean of precision and Recall taking both metrics into account. Support shows the actual frequency of a class or category in our dataset. The micro average (Micro avg) shows the average sum of the true and false predictions of different classes or categories in our dataset. While the macro average (Macro avg) indicates the simple average scores of each target classes independently. The weighted average (Weighted avg) is the average of each class in the dataset that corresponds to their proportion. The values 1 and 0 represent the two types of MR image in our dataset which are non-tumor affected and tumor affected images respectively. The accuracy and the loss plots given in the Figures 8-9 show that the model was learning and had an effective training performance without encountering any kind of over-fitting problems. It can be seen clearly in the Figure 9 that the model perfectly converged to the global minima on the gradient decent curve after going through all the epochs.

Figures 8-9 also show that the activation function used to prevent the vanishing gradient issue has worked adequately. A vanishing gradient is one of the major challenges when it comes to deep neural networks and it mainly occurs in a very important process in deep learning known as backpropagation.

Figure 8

The accuracy plot

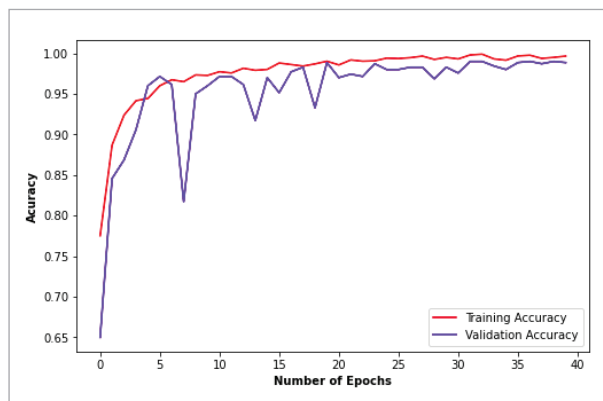
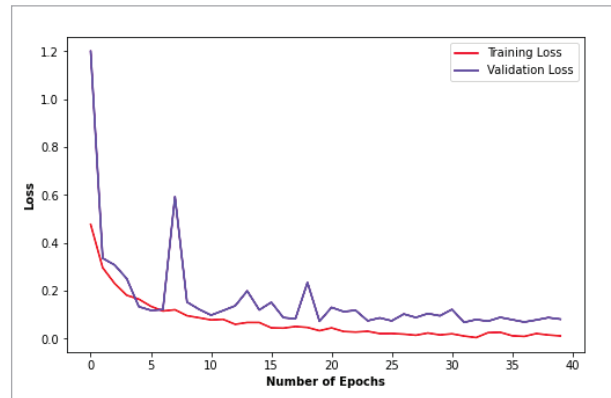


Figure 9

The loss plot



Backpropagation is the process where the weights of the network are updated in response to the output of the loss function after each epoch during the training of the model. Updating the weights helps to reduce the loss of the model in cooperation with the Adam optimization algorithm.

A comparative study was conducted to show the performance of our method over the recent methods in this topic using the similar data structure. This comparison is demonstrated in Table 5.

Table 5

Performance comparison of our method and the similar methods using MRI data set

Author	Classified Method	Accuracy
Deepak & Ameer, 2020 [10]	Siamese Neural Network (GoogLeNet)	97.64%
Cinar & Yildirim, 2020 [9]	Hybrid CNN (Resnet50)	97.2%
Preethi & Aishwarya, 2021 [30]	Optimal DNN and Spider Monkey Optimization	99.3%
Kharrat et al., 2011 [20]	Wavelet Transform and Support Vector Machine	98.14%
Diaz-Pernas et al., 2021 [11]	Multiscale CNN	97.3%
Hemanth et al., 2018 [15]	Modified Deep CNN	96.4%
Paul et al., 2017 [29]	Convolutional Neural Network	91.43%
Proposed method	Deep Transfer Learning (AlexNet)	99.62%

Deepak and Ameer designed a Siamese Neural Network to represent GoogLeNet encodings via transfer learning and achieved 97.64% mean average precision. Cinar and Yildirim obtained 97.2% accuracy using CNN and ResNet50 architecture. Preethi and Ashwarya used optimal deep neural network by applying Spider Monkey Optimization to optimally selecting the weights and obtained as high as 99.3% accuracy. Kharrat et al. obtained about 98% accuracy using wavelet transform and support vector machines. Diaz-Pernas et al. recently used multiscale CNN and obtained 97.3% accuracy. Hemanth et al. used modified deep CNN by obtaining 96.4% accuracy. Paul et al. used neural networks and obtained 91.43% accuracy. As it can be seen from the classification methods, various techniques have been used for classifying the brain tumor images. The modifications or hybrid versions of CNN are the majority of these methods in the Table. Despite of these effective modifications applied on CNN, our AlexNet based-modified CNN method stands out as being the efficient in terms of performance accuracy among the previous related works on this topic. Furthermore, a self-comparison was also performed where we trained and evaluated two different transfer learning models, namely, VGG16 and ResNet50 alongside the proposed algorithm. The results of these two deep learning algorithms were compared to our proposed algorithm using their respective confusion matrices and their overall accuracy scores which are shown in Figures 10-11 with Tables 6-7.

The accuracy score of VGG19 was 99.4%. This model performed sufficiently considering that only 5 of the images were misclassified out of 7858 images.

This algorithm classified 2 samples as tumor affected and 3 samples as non-tumor affected, while in fact it is the opposite in both cases. In addition, 2 of the image samples were skipped by the model during training and that is because the model could not classify those images, whether they belonged to the non-tumor affected or tumor affected dataset.

Regarding the results obtained by ResNet50 model, the overall accuracy score was 98.09%. This indicated that this model performed well on the data set. The confusion matrix in Figure 11 shows that out of the entire dataset, this algorithm has only misclassified 11 images. It indicated that 3 samples were classified

Figure 10

The confusion matrix for VGG19

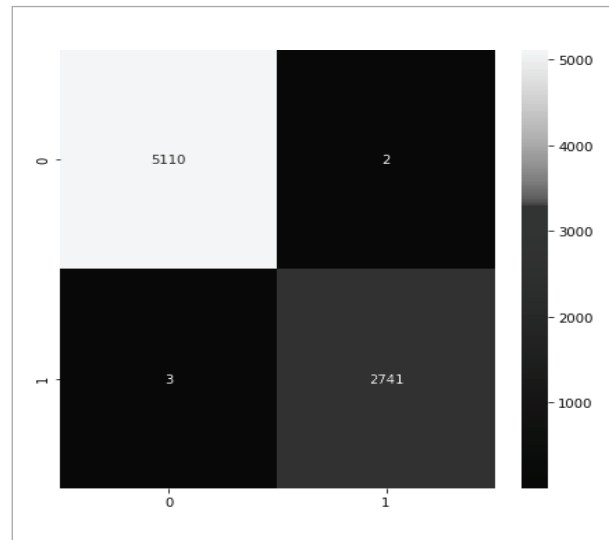


Table 6

VGG19 Confusion Matrix Parameters

True Positive (TP)	False Positive (FP)	True Negative (TN)	False Negative (FN)
5110 samples	2 samples	2741 samples	3 samples

Table 7

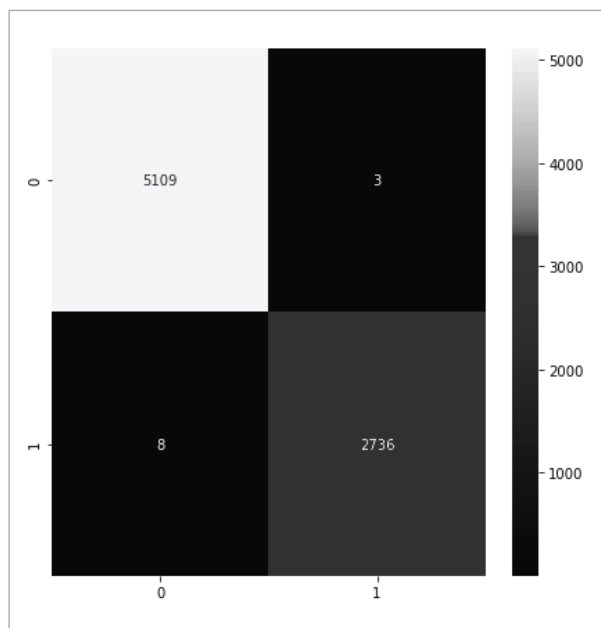
ResNet50 Confusion Matrix Parameters

True Positive (TP)	False Positive (FP)	True Negative (TN)	False Negative (FN)
5109 samples	3 samples	2736 samples	8 samples

as non-tumor affected and 8 samples were classified as tumor affected, while in reality, it is the opposite for these two scenarios. However, the same scenario happened in the ResNet50 model during the training as in the VGG19 model, where two of the image samples were skipped by the model because the model could not identify whether they belonged to the non-tumor affected or tumor-affected dataset. As an overall observation we can say that the proposed model performed better than these two models. Although VGG19 and ResNet50 performed well for the same

Figure 11

The confusion matrix for ResNet50



data set, in such critical problems like brain tumor classification, accuracy is one of the most decisive performance scale. Considering this, it can be said that our model performed better than the compared models significantly.

References

1. Abdulkarim, H. A., Abdul Razak, M. A., Sudirman, R., Ramli, N. A Deep Learning AlexNet Model for Classification of Red Blood Cells in Sickle Cell Anemia. *IAES International Journal of Artificial Intelligence (IJ-AD)*, 2020, 9(2), 221. <https://doi.org/10.11591/ijai.v9.i2.pp221-228>
2. Abiwinanda, N., Hanif, M., Hesaputra, S. T., Handayani, A., Mengko, T. R. Brain Tumor Classification Using Convolutional Neural Network. *IFMBE Proceedings*, 2018, 183-189. https://doi.org/10.1007/978-981-10-9035-6_33
3. Afshar, P., Plataniotis, K. N., Mohammadi, A. Capsule Networks' Interpretability for Brain Tumor Classification Via Radiomics Analyses, *IEEE International Conference on Image Processing (ICIP)*, 2019, 3816-3820. <https://doi.org/10.1109/ICIP.2019.8803615>
4. Alom, M. Z., Taha, T. M., Yakopcic, C., Westberg, S., Sidike, P., Nasrin, M. S., Asari, V. K. The History Began From Alexnet: A Comprehensive Survey on Deep Learning Approaches. *arXiv preprint arXiv:1803.01164*, 2018.
5. Alom, M. Z., Taha, T. M., Yakopcic, C., Westberg, S., Sidike, P., Nasrin, M. S., Hasan, M., Van Essen, B. C., Awwal, A. A. S., Asari, V. K. A State-of-the-Art Survey on Deep Learning Theory and Architectures. *Electronics*, 2019, 8(3), 292. <https://doi.org/10.3390/electronics8030292>
6. Alqudah, A. M., Alquraan, H., Qasmieh, I. A., Alqudah, A., Al-Sharu, W. Brain Tumor Classification Using Deep Learning Technique - A Comparison Between Cropped, Uncropped, and Segmented Lesion Images with Different Sizes. *International Journal of Advanced Trends in Computer Science and Engineering*, 2019, 8(6), 3684-3691. <https://doi.org/10.30534/ijatcse/2019/155862019>

4. Conclusions

This paper introduced a new model derived by the combination of CNN and AlexNet for detecting and classifying brain tumors in an enhanced MR image dataset. The proposed algorithm has demonstrated excellent performance in extracting the most important features of the images as well as identifying the key relevant points on the images before they are fed into the fully-connected network for classification. The proposed architecture is important in classifying tumors in brain MR images since it enables radiologists to make quicker and more accurate decisions in diagnosing a patient. When the predicted labels were compared with the ground truth labels, we observed that there was no overlapping of data points during training and the model was able to find all the patterns within the dataset. This model belongs to the category of easy to implement on standard contemporary personal computers and there is no need for physical data engineering or physical image processing, hence those tasks are performed by the network's pre-trained parameters. The results of the evaluation metrics of the model and both accuracy and loss plots prove that the proposed algorithm learns and evaluates the trend of the data successfully, especially in brain tumor classification where the performance and accuracy are crucial.

7. Badža, M. M., Barjaktarović, M. Classification of Brain Tumors from MRI Images Using a Convolutional Neural Network. *Applied Sciences*, 2020, 10(6), 1999. <https://doi.org/10.3390/app10061999>
8. Cheng, J., Huang, W., Cao, S., Yang, R., Yang, W., Yun, Z., Wang, Z., Feng, Q. Correction: Enhanced Performance of Brain Tumor Classification via Tumor Region Augmentation and Partition. *PLOS ONE*, 2015, 10(12), 0144479. <https://doi.org/10.1371/journal.pone.0144479>
9. Çınar, A., Yildirim, M. Detection of Tumors on Brain MRI Images Using the Hybrid Convolutional Neural Network Architecture. *Medical Hypotheses*, 2020, 139, 109684. <https://doi.org/10.1016/j.mehy.2020.109684>
10. Deepak, S., Ameer, P. Retrieval of brain MRI with Tumor Using Contrastive Loss Based Similarity on GoogleNet Encodings. *Computers in Biology and Medicine*, 2020, 125, 103993. <https://doi.org/10.1016/j.compbiomed.2020.103993>
11. Díaz-Pernas, F. J., Martínez-Zarzuela, M., Antón-Rodríguez, M., González-Ortega, D. A Deep Learning Approach for Brain Tumor Classification and Segmentation Using a Multiscale Convolutional Neural Network, *Healthcare*, 2021, 9(2), 153. <https://doi.org/10.3390/healthcare9020153>
12. Fabelo, H., Halicek, M., Ortega, S., Shahedi, M., Szolna, A., Piñeiro, J.F., Sosa, C., O'Shanahan, A.J., Bisshopp, S., Espino, C., Márquez, M. Deep Learning-Based Framework for in Vivo Identification of Glioblastoma Tumor Using Hyperspectral Images of Human Brain. *Sensors*, 2019, 19(4), 920. <https://doi.org/10.3390/s19040920>
13. Ghassemi, N., Shoeibi, A., Rouhani, M. Deep Neural Network with Generative Adversarial Networks Pre-Training for Brain Tumor Classification Based on MR Images. *Biomedical Signal Processing and Control*, 2020, 57, 101678. <https://doi.org/10.1016/j.bspc.2019.101678>
14. Gumaei, A., Hassan, M. M., Hassan, M. R., Alelaiwi, A., Fortino, G. A Hybrid Feature Extraction Method with Regularized Extreme Learning Machine for Brain Tumor Classification, *IEEE Access*, 2019, 7, 36266-36273. <https://doi.org/10.1109/ACCESS.2019.2904145>
15. Hemanth, D. J., Anitha, J., Naaji, A., Geman, O., Popescu, D. E., Hoang Son, L. A Modified Deep Convolutional Neural Network for Abnormal Brain Image Classification. *IEEE Access*, 2019, 7, 4275-4283. <https://doi.org/10.1109/ACCESS.2018.2885639>
16. <https://www.kaggle.com/datasets?search=MRI+-brain+tumor+dataset&datasetsOnly=true>
17. Irmak, E. Multi-classification of Brain Tumor MRI Images Using Deep Convolutional Neural Network with Fully Optimized Framework. *Iranian Journal of Science and Technology, Transactions of Electrical Engineering*, 2021, 45(3), 1015-1036. <https://doi.org/10.1007/s40998-021-00426-9>
18. Ismael, M. R., Abdel-Qader, I. Brain Tumor Classification via Statistical Features and Back-Propagation Neural Network, *IEEE International Conference on Electro/Information Technology*, 2018, 0252-0257. <https://doi.org/10.1109/EIT.2018.8500308>
19. Jais, I. K. M., Ismail, A. R., Nisa, S. Q. Adam Optimization Algorithm for Wide and Deep Neural Network. *Knowledge Engineering and Data Science*, 2019, 2(1), 41-46. <https://doi.org/10.17977/um018v2i12019p41-46>
20. Kharrat, A., Gasmi, K., Ben Messaoud, M., Benamrane, N., Abid, M. Medical Image Classification Using an Optimal Feature Extraction Algorithm and a Supervised Classifier Technique, *International Journal of Software Science and Computational Intelligence*, 2011, 3(2), 19-33. <https://doi.org/10.4018/jssci.2011040102>
21. Khun, M., Johnson, K. *Applied Predictive Modelling*, Springer, 2013. <https://doi.org/10.1007/978-1-4614-6849-3>
22. Krizhevsky, A., Sutskever, I., Hinton, G. E. ImageNet Classification with Deep Convolutional Neural Networks. *Communications of the ACM*, 2017, 60(6), 84-90. <https://doi.org/10.1145/3065386>
23. Kumar P, Vijayakumar B. Brain Tumour Mri Image Segmentation and Classification Using by PCA and RBF Kernel Based Support Vector Machine. *Middle-East Journal of Scientific Research*, 2015, 23(9), 2106-16.
24. Kumar, R. L., Kakarla, J., Isunuri, B. V., Singh, M. Multi-class Brain Tumor Classification Using Residual Network and Global Maximum Pooling. *Multimedia Tools and Applications*, 2021, 80(9), 13429-13438. <https://doi.org/10.1007/s11042-020-10335-4>
25. LeCun, Y., Bengio, Y., Hinton, G. Deep Learning. *Nature*, 2014, 521(7553), 436-444. <https://doi.org/10.1038/nature14539>
26. Lu, S., Lu, Z., Zhang, Y. D. Pathological Brain Detection Based on AlexNet and Transfer Learning. *Journal of Computational Science*, 2019, 30, 41-47. <https://doi.org/10.1016/j.jocs.2018.11.008>
27. Mehmood, A., Ali, A., Application of Deep Reinforcement Learning for Tracking Control of 3WD Omnidirectional Mobile Robot. *Information Technology and Control*, 2021, 24, 50(3), 507-21. <https://doi.org/10.5755/j01.itc.50.3.25979>

28. Pashaei, A., Sajedi, H., Jazayeri, N. Brain Tumor Classification via Convolutional Neural Network and Extreme Learning Machines. 2018 8th International Conference on Computer and Knowledge Engineering (ICCKE). <https://doi.org/10.1109/ICCKE.2018.8566571>
29. Paul, J. S., Plassard, A. J., Landman, B. A., Fabbri, D. Deep Learning for Brain Tumor Classification. Medical Imaging 2017: Biomedical Applications in Molecular, Structural, and Functional Imaging. <https://doi.org/10.1117/12.2254195>
30. Preethi, S., Aishwarya, P. An Efficient Wavelet-Based Image Fusion for Brain Tumor Detection and Segmentation Over PET and MRI Image. Multimedia Tools and Applications, 2021, 80(10), 14789-14806. <https://doi.org/10.1007/s11042-021-10538-3>
31. Rehman, A., Khan, M. A., Saba, T., Mehmood, Z., Tariq, U., Ayesha, N. Microscopic Brain Tumor Detection and Classification Using 3D CNN and Feature Selection Architecture. Microscopy Research and Technique, 2020, 84(1), 133-149. <https://doi.org/10.1002/jemt.23597>
32. Russel, S., Norvig, P. AI: A Modern Approach. Pearson Prentice Hall, 3rd Edition, 2009.
33. Shoieb, D. Computer-Aided Model for Skin Diagnosis Using Deep Learning. Indian Journal of Image and Graphics, 2016, 4(2), 122-129. <https://doi.org/10.18178/joig.4.2.122-129>
34. Sultan, H. H., Salem, N. M., Al-Atabany, W. Multi-Classification of Brain Tumor Images Using Deep Neural Network. IEEE Access, 2019, 7, 69215-69225. <https://doi.org/10.1109/ACCESS.2019.2919122>
35. Sun, G., Wang, Z., Zhao, J. Automatic Text Summarization Using Deep Reinforcement Learning and Beyond, Information Technology and Control, 2021, 24, 50(3), 458-9. <https://doi.org/10.5755/j01.itc.50.3.28047>
36. Swati, Z.N.K., Zhao, Q., Kabir, M., Ali, F., Ali, Z., Ahmed, S., Lu, J. Brain Tumor Classification for MR Images Using Transfer Learning and Fine-tuning. Computerized Medical Imaging and Graphics, 2019, 75, 34-46. <https://doi.org/10.1016/j.compmedimag.2019.05.001>

